Геология и геофизика, *т. 65, № 4, с. 601—612*, DOI: 10.15372/GiG2023171, EDN: TFLXDW
Поступила в редакцию 16.03.2023, принята в печать 01.09.2023 *Опубликована онлайн: 03.09.2024*

УДК 553.982(549)

ИССЛЕДОВАНИЕ НЕФТЕГЕНЕРАЦИОННОГО ПОТЕНЦИАЛА МАТЕРИНСКИХ ПОРОД И ПОРОД-КОЛЛЕКТОРОВ РАННЕЭОЦЕНОВЫХ И ПАЛЕОЦЕНОВЫХ ТОЛЩ БАССЕЙНА ПЛАТФОРМЫ ПЕНДЖАБ, ПАКИСТАН: ГЕОХИМИЧЕСКИЙ И ПЕТРОФИЗИЧЕСКИЙ ПОДХОД

Сайед Билавал Али Шах

Университет Малайи, Куала-Лумпур, 50603, Малайзия

Исследование раннеэоценовых и палеоценовых отложений платформы Пенджаб в Пакистане включало комплексный анализ с использованием передовых геохимических и петрофизических методов. В данной работе проведена оценка нефтематеринского потенциала четырех пластов: Наммал, Сакесар раннеэоценового возраста и Дунган, Раникот палеоценового возраста. Для пласта Сакесар, сложенного породами-коллекторами, была сделана интерпретация кабельных каротажных диаграмм для оценки его ключевых петрофизических свойств — пористости, водонасыщенности и нефтенасыщенности. В геохимических исследованиях основное внимание было уделено определению содержания общего органического углерода (TOC) и Rock-Eval-пиролизу двадцати одной пробы бурового шлама. В этих образцах содержания TOC изменялись в диапазоне от 0.21 до 2.04 мас. %, а значения S_2 — в диапазоне от 0.09 до 2.14 мг УВ/г породы. Анализ показал, что все образцы относятся к зоне незрелой нефти с керогеном типов II/III и III, что указывает на ограниченный нефтегенерационный потенциал пород. Результаты исследований позволяют предположить ограниченное образование углеводородов в этих пластах. Петрофизический анализ для пласта Сакесар показал среднюю пористость 11.2 %, водонасыщенность 32.58 % и нефтенасыщенность 67.42 %, что позволяет отнести его к коллектору с умеренным или высоким углеводородным потенциалом. Данное исследование освещает сложные геохимические и петрофизические характеристики этих пластов. Пласт Сакесар демонстрирует коллекторские свойства, в то время как пласты Наммаль, Дунган и Раникот имеют ограниченный углеводородный потенциал. Рассмотрение этих пластов в качестве источников углеводородов требует обоснования.

Бассейн Среднего Инда, пласт Сакесар, нефтематеринские породы, породы-коллекторы, петрофизический анализ

INVESTIGATION OF SOURCE AND RESERVOIR ROCK PETROLEUM GENERATIVE POTENTIAL OF EARLY EOCENE AND PALEOCENE SEQUENCES OF THE PUNJAB PLATFORM BASIN, PAKISTAN: A GEOCHEMICAL AND PETROPHYSICAL APPROACH

Syed Bilawal Ali Shah

Investigating Early Eocene and Paleocene deposits within the Punjab Platform, Pakistan, involved comprehensive analysis using advanced geochemical and petrophysical techniques. This study evaluates the source potential of three formations: Nammal and Sakesar of Early Eocene age and Dungan and Ranikot of Palaeocene age. The Sakesar Formation, a reservoir rock, was evaluated through interpretation of wireline logs to estimate key petrophysical properties—porosity, water saturation, and hydrocarbon saturation. Geochemical investigations focused on total organic carbon content and Rock-Eval pyrolysis of twenty-one cutting samples from a well. These samples displayed TOC values ranging from 0.21 to 2.04 wt.% and S2 values ranging from 0.09 to 2.14 mg HC/g rock. Analysis positioned all samples within the immature window zone with Type II/III and Type III kerogen, suggesting limited generative potential. Findings suggest limited hydrocarbon generation from these formations. Petrophysical analysis indicated average porosity of 11.2%, water saturation of 32.58%, and hydrocarbon saturation of 67.42% for the Sakesar Formation, categorizing it as average to good reservoir potential. This study highlights complex geochemical and petrophysical characteristics of these formations. While Sakesar shows promising reservoir qualities, significant hydrocarbon generation potential from Nammal, Dungan, and Ranikot formations is constrained. Informed decision-making is crucial when considering these formations as hydrocarbon sources.

Middle Indus Basin, Sakesar Formation, source and reservoir rock, petrophysical analysis

✉e-mail: bilawalshah22@yahoo.com

INTRODUCTION

The Punjab Platform, situated within the Middle Indus Basin, encompasses a tripartite geological structure comprising the Punjab Platform itself, the Sulaiman Fold Belt, and the Sulaiman Depression. Our research is centered in the Punjab Platform basin, specifically within the confines of Jhang District, Punjab Province, situated at coordinates 30°49'21.60"N latitude and 71°55'49.10"E longitude. Geologically, this region exhibits a distinctive westward-dipping basin configuration (Fig. 1), representing the least altered portion of the Middle Indus Basin. The Punjab Platform gracefully descends toward the Sulaiman Depression, where it eventually converges. Notably, the northern boundary is demarcated by the Sargodha High, while the southern boundary is characterized by the Mari High (Kadri, 1995; Shah and Shah, 2021; Peng et al., 2022; Dang et al., 2023).

Significant attention has been drawn to this area due to the identification of rock formations with promising gas potential (Raza, 1973; Shah et al., 2019; Zhang et al., 2022a; Zhan et al., 2022). The presence of organic-rich materials within the deposits of the Punjab Platform Basin, as reported by Shah et al. (2019), underscores the necessity to reevaluate the source and reservoir rock characteristics of the Early Eocene Nammal and Sakesar formations, as well as the Paleocene Dungan and Ranikot formations. Our study is primarily focused on these aspects. Additionally, the Middle Indus Basin is renowned for its source rocks, including the Shinwari Formation shales, Ranikot, Kingriali, Lumshiwal, Samana Suk, and Chichali formations (Shah, 2023a; Ma et al., 2023; Yang et al., 2023a; Yuan et al., 2023). It's imperative to note that recent discoveries of oil and gas fields in close proximity have garnered the interest of petroleum companies. Specifically, oil reserves have been uncovered in India within this platform, and Pakistan has witnessed the discovery of gas reserves in the Panjpir Oilfield (Shah et al., 2019; He et al., 2021; Li et al., 2022a; Zhang et al., 2022b).

The distinctive contribution of this research lies in the comprehensive analysis of well cutting samples, encompassing the evaluation of source rock generation potential, thermal maturity assessment, kerogen type identification, and petrophysical analysis for a profound understanding of reservoir rock properties and their potential. This research also stands out for its simultaneous employment of two distinct methodologies to assess the pivotal properties of the petroleum system, namely source and reservoir rock properties, representing a novel approach in this field.

Wireline log data serve as invaluable tools in transforming raw log data into actionable insights regarding subsurface hydrocarbon reserves (Quijada and Stewart, 2007; Xu et al., 2022a; Yu et al., 2021; Zheng et al., 2023). These logs provide critical information pertaining to rock properties, including permeability, porosity, and lithological composition, all of which are paramount in the realm of oil and gas exploration (Asquith et al., 2004; Xu et al., 2021, 2022b). In this study, we apply the qualitative reservoir description criteria established by Rider

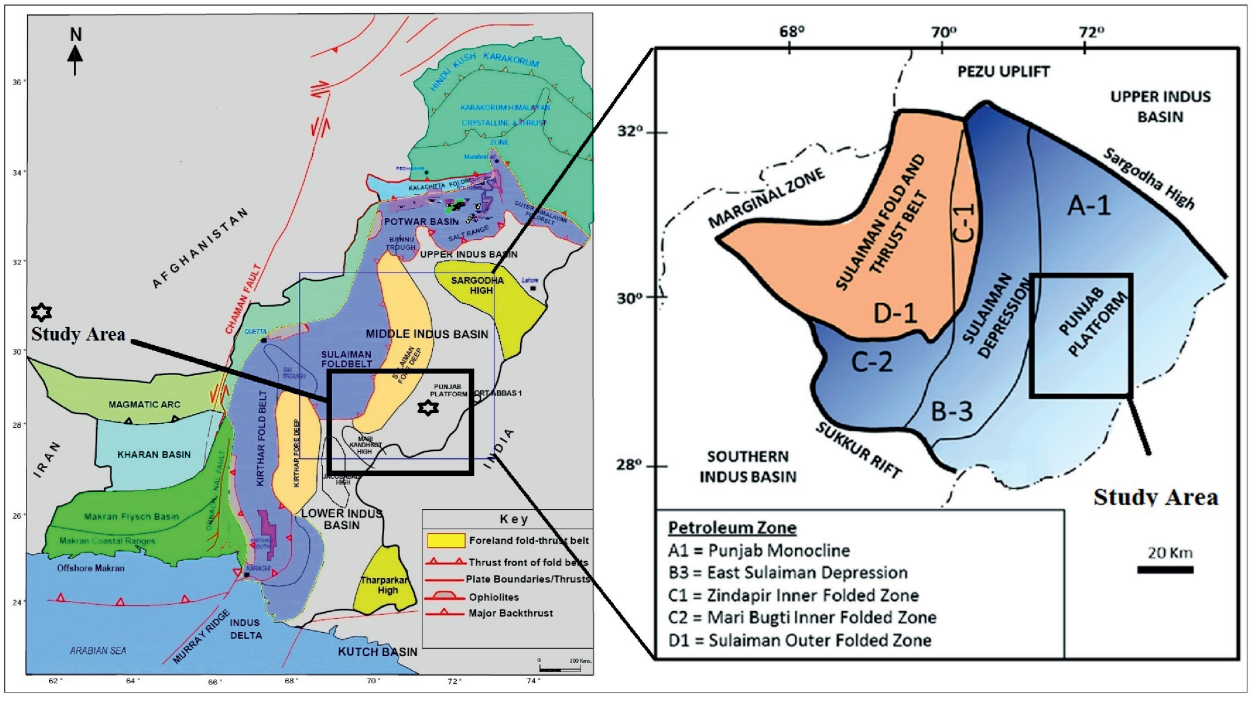

Fig. 1. Map displaying the Punjab platform with surroundings (Huang et al., 2021; Wu et al., 2022; Shah et al., 2023b; Wang et al., 2023).

(1986) and Shah and Abdullah (2017). Figure 1 illustrates the geographical scope of our investigation, while Table 1 delineates Rider's (1986) and Shah et al. (2023a) criteria for qualitative reservoir description.

This research endeavor aims to unravel the intricate geological and hydrocarbon potential of the Punjab Platform Basin, underpinned by a holistic approach that combines well cutting sample analysis and wireline logs to offer comprehensive insights into the source and reservoir rock properties, thereby presenting a novel contribution to the field of petroleum exploration.

Table 1. **Reservoirs' porosity as described qualitatively by Rider (1986)**

Average Porosity with Qualitative Description
Porosity ranging from 0 to 5% is considered Negligible
Porosity ranging from 5 to 10% is considered Poor
Porosity ranging from 10 to 20% is considered Good
Porosity ranging from 20 to 30% is considered Very good
Porosity greater >30% is considered Excellent

GEOLOGICAL SETTING

During the late Proterozoic era, the Indian Plate underwent a process of rifting, resulting in the deposition of Infra-Cambrian sediments atop the Precambrian basement. Within the context of the Punjab Platform, the second phase of rifting presents a complex challenge in terms of differentiation, primarily due to the influence of drag forces acting on the geological structures (Li et al., 2022b; Ren et al., 2022a; Shah et al., 2023a). Nonetheless, discernible indications of the second rifting phase have been unveiled through seismic profiling, showcasing instances of Cretaceous strata displacement attributed to normal fault mechanisms. This dynamic geological setting is further shaped by the ongoing tectonic interaction involving the Indian Plate, encompassing both collision and subduction processes, which collectively influence the basin's structural evolution (Shah et al., 2019; Shah and Abdullah, 2017; Li et al., 2023a).

The result of these geological processes is the concealment of alluvium deposits, primarily composed of silt, clay, and sand sedimentary rocks, which are not exposed in the region. The geological significance of this basin has been underscored by recent discoveries of oil and gas reserves in adjacent areas, subsequently piquing the interest of petroleum companies. Notably, oil reservoirs have been identified on this platform in India, while gas reserves have been successfully located in the Panjpir oilfield in Pakistan (Zhou et al., 2021a; Ran et al., 2023; Shah, 2023b).

The stratigraphic framework of the Punjab Platform has been meticulously established through comprehensive drilling data analysis. This basin predominantly consists of marine sedimentary rocks spanning from the Paleozoic to the Cenozoic era. Noteworthy similarities in the Lower Triassic stratigraphy between the Punjab Platform and the Potwar basins are observed in the southern region, exemplifying their geological affinity (Raza et al., 2008; Shah, 2009; Yang et al., 2022; Li et al., 2023b). Within this stratigraphic context, several formations, including the Shinwari Formation shales, Ranikot, Kingriali, Lumshiwal, Samana Suk, and Chichali formations, have earned recognition as proven source rocks within the Middle Indus Basin (Shah and Abdullah, 2016; Sun et al., 2023a; Xiao et al., 2023) (Table 2).

This intricate geological setting, characterized by its historical rifting, ongoing tectonic dynamics, and concealed sedimentary deposits, forms the backdrop against which our research endeavors to explore and understand the petroleum potential of the Punjab Platform Basin.

MATERIAL AND METHODS

In this research, well cutting samples were systematically collected at intervals ranging from 10 to 30 m, ensuring comprehensive coverage of the stratigraphic sequence. The sediments under scrutiny encompass geologic epochs including the Early Eocene, Paleocene, and Cretaceous periods, as detailed in Table 5 for a comprehensive overview of the sampled materials.

To evaluate the petrophysical attributes pertinent to the reservoir potential of the Sakesar Formation, a dataset of well logs obtained from Well A was judiciously employed. These well log data, vital to our study, were graciously provided by the Directorate General Petroleum Concessions, Islamabad, Pakistan. The analytical framework adopted here drew upon an array of established methodologies, including those outlined in Shah et al. (2023b), Zahid et al. (2014), and Hartmann and Beaumont (1999). This multi-faceted approach leveraged a suite of wireline logs, including Neutron, Resistivity, Density, Gamma Ray, and Spontaneous Potential logs, each playing a pivotal role in elucidating critical petrophysical parameters. From these meticulously analyzed logs, we computed essential attributes such as porosity, formation water resistivity, water saturation, and hydrocarbon saturation. These parameters collectively constitute a fundamental cornerstone in the comprehensive assessment of the hydrocarbon potential intrinsic to reservoir rocks, shedding light on the intricate subsurface dynamics crucial to our study.

ORGANIC GEOCHEMICAL ANALYSIS

The organic geochemical analysis conducted in this study entailed a meticulous examination of 21 well cutting samples, meticulously collected at intervals spanning 10 to 30 m, originating from formations dating back to the Early Eocene and Paleocene epochs. Specifically, these samples were sourced from the Nammal Formation (Early Eocene) as well as the Dungan and Ranikot formations (Paleocene).

The collected cutting samples underwent a rigorous preparation process. Initially, they were subjected to crushing, reducing their particle size to below 200 mesh, followed by further grinding to achieve a finely granulated state. To assess the organic content, we employed LECO elemental analyzers CS-125 equipment for precise Total Organic Carbon (TOC) measurements. Moreover, the evaluation encompassed pyrolysis analysis employing the Rock-Eval VI instrument. Approximately 100 mg of the finely crushed samples were subjected to pyrolysis within a helium atmosphere, maintained at a temperature of 600 °C. Pyrolysis, a pivotal technique, yielded three paramount parameters for analysis:

S1, serving as an indicator of the quantity of free petroleum,

S2, offering insights into the quantity of hydrocarbons generated through thermal cracking, and

T_{max}, denoting the maximum temperature reached during the pyrolysis process (Shah and Shah, 2021).

Furthermore, to provide a comprehensive assessment, our analysis encompassed the computation of additional critical parameters, including:

OI (oxygen index), elucidating the oxygen content within the organic matter,

HI (hydrogen index), elucidating the hydrogen content within the organic matter, and

IP (production index), shedding light on the hydrocarbon generation potential of the samples.

This comprehensive organic geochemical analysis contributes invaluable insights into the composition and hydrocarbon potential of the studied formations, facilitating a deeper understanding of their geological and petroleum prospects.

WELL LOG ANALYSIS

Procedure for extracting various parameters from well logs are:

The parameters that were directly read from the log track are:

1. Formation depth (in ft.);
2. (NPHI) Neutron porosity (0.45 to –0.15 scale);
3. (LLD) Bulk resistivity of the formation (0–2000 Ohm·m scale);
4. (SP) Spontaneous potential (0–100 mv scale);
5. (RHOB) Bulk density of formation (1.95 to 2.95 scale).

HYDROCARBON SATURATION (SH)

Schlumberger log interpretation charts were utilised in conjunction with multiple equations to determine certain required data in the Sakesar Formation encountered well A for estimating reservoir potential. The graphs and equations were used together in the following flow:

1. Wireline log report shows a bottom-hole temperature of 180 °F and a surface temperature of 72 °F which were utilised in the equation (Fig. 2). Following equation was used to calculate the temperature of the formation:

$$\mathrm{Tf} = \mathrm{Ts} + \mathrm{Df}\left(\frac{BHT - TS}{TD}\right).$$

2. (R_{mf}) Mud Filtrate Resistivity and (R_m) Resistivity of Mud at Formation Temperature were corrected. (Fig. 4).

3. Self-Potential was directly determined from the log chart SP curve.

4. The value of the R_{mf}/R_{we} ratio was measured using Fig. 5.

5. R_{we} was calculated by dividing the corrected R_{mf} value by the R_{mf}/R_{we} value ratio.

6. The equation for R_{we} is:

$$R\mathrm{we} = \left(\frac{R\mathrm{mfeq}}{\left(\frac{R\mathrm{mfeq}}{R\mathrm{we}}\right)}\right).$$

7. $R_{we} = R_{mfeq}/(R_{mfeq}/R_{we})$

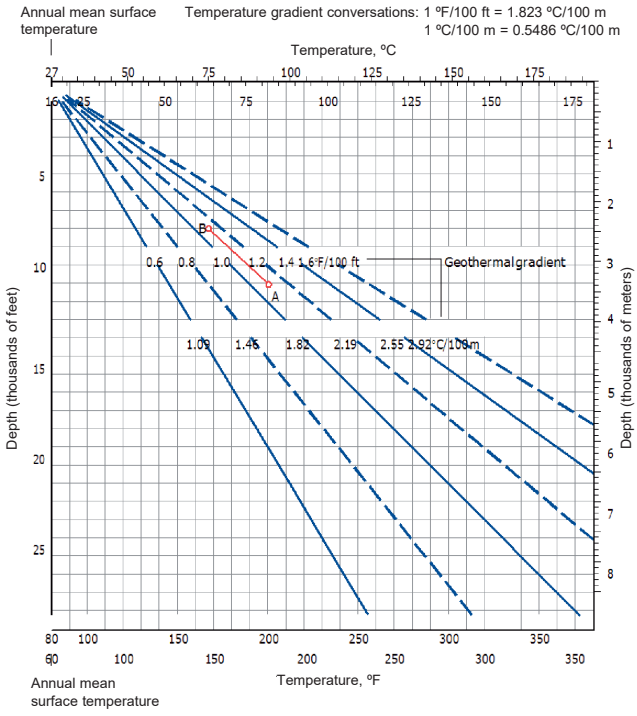

Fig. 2. Temperature of the formation at various depths.

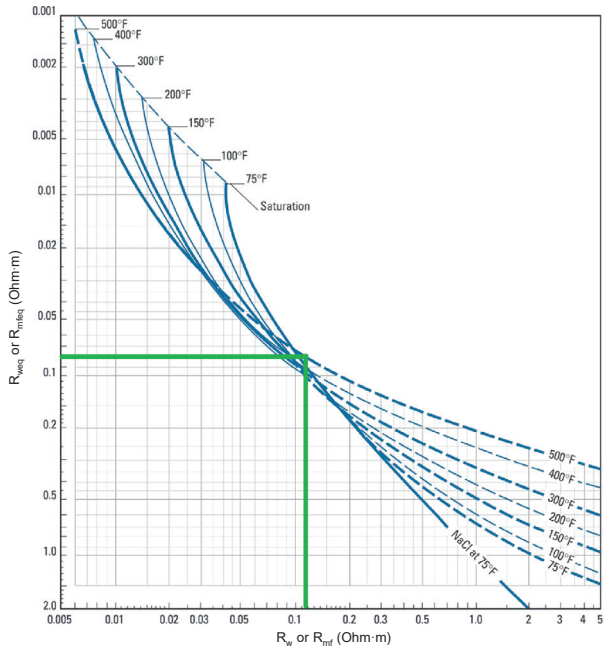

Fig. 3. R_w determined by determining R_{we} (Schlumberger, 1977).

8. Figure 3 was used to convert R_{we} to R_w, and the correct R_{we} value was determined using the R_{we} value derived in step 5.

9. Archie's equation was used to estimate water saturation.

$$S_w = \sqrt{\frac{R_w}{\phi^m \cdot R_t}}.$$

10. Following equation can be used to estimate the saturation of a hydrocarbon at a particular temperature: SH = 1–Sw.

After obtaining the mud filtrate resistivity values, they were used in Fig. 3 to convert them to equivalent mud filtrate resistivity values. The equivalent mud filtrate resistivity values were then utilised in step 6's calculation to get equivalent water resistivity. This equivalent water resistivity were then converted to water resistivity, which was then utilised in Archie's equation to calculate water saturation.

Because the mud filtrate resistivity in the log header was determined at surface temperature, it needs to be corrected at formation temperature for each value at a certain depth to determine the mud filtrate resistivity at formation temperature Fig. 4 was used for this correction.

RESULTS AND DISCUSSION

Organic matter content and generative potential: The characterization of organic matter within source sediments and its capacity for hydrocarbon generation is pivotal in quantifying both the abundance of organic material and its potential to yield petroleum upon thermal maturation (Peters and Cassa, 1994; Hunt, 1996; Yin et al., 2023). In this investigation, we assessed the hydrocarbon generation potential of the analyzed sediments through organic geochemical analyses, including TOC content, as well as S1 and S2 values derived from pyrolysis assessments. The formations under scrutiny for their source rock potential are the Early Eocene Nammal Formation, the Paleocene Dungan Formation, and the Ranikot Formation. Average results are summarized in Table 3, while detailed sample data can be found in Table 5.

Typically, the organic richness of rock is gauged by the TOC weight percentage (%). According to Hunt (1996), a clastic rock must exhibit a TOC of at least 1.0% to qualify as a potential source rock. Within the Nammal Formation sediments, TOC content varies from 0.21 to 2.04%, with an average of 1.02% TOC. The Dungan Formation sediments show an average TOC of 0.52% and a range of 0.45–0.56% TOC. As for the Ranikot

Table 2. **General stratigraphy of the Punjab Platform Basin (Zhou et al., 2021b; Shah et al., 2023a; Sun et al., 2023b)**

Formation	Lithology	Age	Top depth, m	Bottom depth, m
Nagri	Sandstone	Pliocene	16	600
Chinji	Sandstone and clay	Miocene	600	1269
Sakesar	Limestone	Eocene	1269	1300
Nammal	Shale and marl	Early Eocene	1300	1442
Dunghan	Limestone	Paleocene	1442	1453
Ranikot	Limestone and shale	Paleocene	1453	1484
Lumshiwal	Shale	Cretaceous	1484	1624
Chichali	Silt stone and sandstone	Jurassic	1624	1659
Samana Suk	Sandstone and limestone	Middle Jurassic	1659	1788
Shinwari	Sandstone and siltstone	Early Jurassic	1788	1864
Datta	Sandstone and shale	Early Jurassic	1864	1889
Kingriali	Shale and limestone	Late Triassic	1889	2033
Tredian	Sandstone	Middle Triassic	2033	2078
Chhidru	Sandstone and limestone	Late Permian	2078	2103
Wargal	limestone	Late Permian	2103	2153
Amb	Silt stone interbeds of sandstone	Early Permian	2153	2180
Sardhai	Shale interbeds of sandstone	Early Permian	2180	2258
Warcha	Shale interbeds of sandstone	Early Permian	2258	2396
Dandot	Shale interbeds of limestone	Early Permian	2396	2440
Tobra	Sandstone and conglomerate	Early Permian	2440	2464
Baghanwala	Shale	Middle Cambrian	2464	2593
Jutana	Dolomite	Early Cambrian	2593	2693
Kussak	Sandstone and siltstone	Early Cambrian	2693	2797
Khewra Sandstone	Shale interbeds of dolomite and siltstone	Early Cambrian	2797	2886
Salt Range	Marl, claystone and siltstone	Precambrian	2886	2902

Formation sediments, they exhibit an average TOC of 0.82%, ranging from 0.48 to 1.63% TOC. The collective analysis suggests that the majority of samples possess a reasonable TOC content. It's worth noting that samples with higher thermal maturity levels would feature higher original TOC values compared to their current values; this relationship follows a decline in TOC content with increasing thermal maturity (Chen et al., 2023; Shah et al., 2023a; Yang et al., 2023b). Of particular importance in pyrolysis assessments is the S2 parameter, which serves as a key indicator of hydrocarbon generative potential (Peters, 1986; Ren et al., 2022b, 2023). As stipulated by Abdullah et al. (2017) and Bordenave et al. (1993), a minimum of 5 mg hydrocarbons per gram of S2 is imperative for favorable petroleum generation capability. Generally, hydrocarbon (S2) yields range from 0.09 to 2.14 mg/g in the Nammal Formation, 1.28 to 1.82 mg/g in the Dungan Formation, and 0.13 to 4.15 mg/g in the Ranikot Formation. A visual representation of the S2 versus TOC relationship is provided in Fig.6, revealing that all formations under consideration exhibit a relatively modest potential for petroleum generation.

Kerogen type (The quality of organic matter). The assessment of kerogen types within the formations relied on the pivotal parameter known as the Hydrogen Index (HI). For the Nammal Formation, HI values ranged from 13 to 404 mg HC/g TOC, while the Dungan Formation exhibited HI values within the range of 227 to 325. The Ranikot Formation recorded HI values spanning from 16 to 255. To further categorize kerogen types, pyrolysis data from the analyzed samples were employed to construct a Van Krevelen diagram, plotting HI against T_{max}. This approach allowed for the classification of kerogen types across all formations. The results

Table 3. **Shows the ranges (min – max) of the values of the indicator of samples**

Formation and number of samples	Depth, m	Petroleum Potential			Maturity of sample	Quality of OM	Kerogen Type	Source rock generative potential
		TOC, wt.%	S1	S2	T_{max} °C	HI		
Nammal (8)	1270–1390	0.21–2.04	0.14–0.85	0.09–2.14	407–427	13–404	Mixed Type II/III and Type III	Poor
Dungan (3)	1430–1450	0.45–0.56	0.10–0.27	1.28–1.82	426–427	227–325		Poor
Ranikot (10)	1455–1510	0.48–1.63	0.18–0.44	0.13–4.15	329–428	16–255		Poor

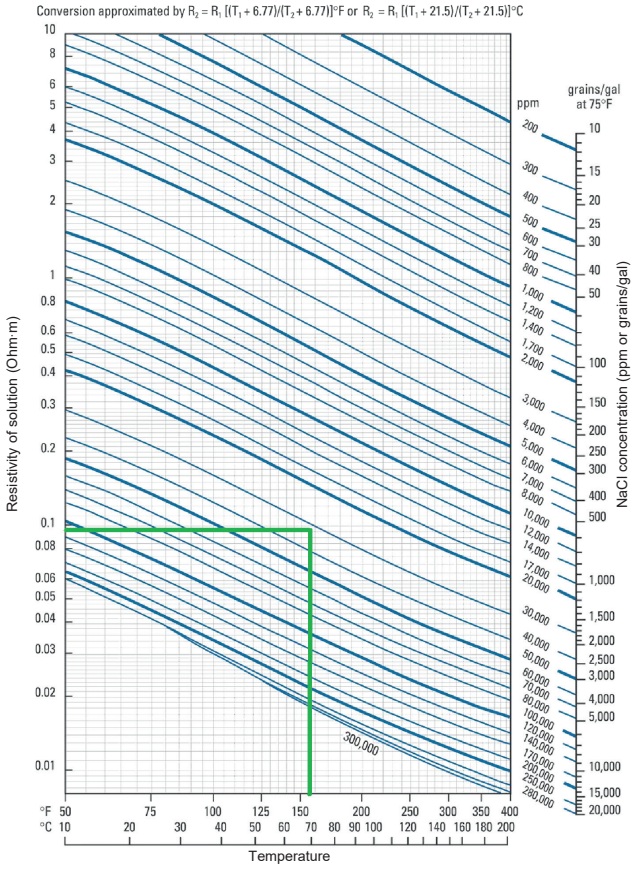

Fig. 4. R_{mf} and R_{we} correction according to temperature (Schlumberger, 1977; Zhou et al., 2021c, d).

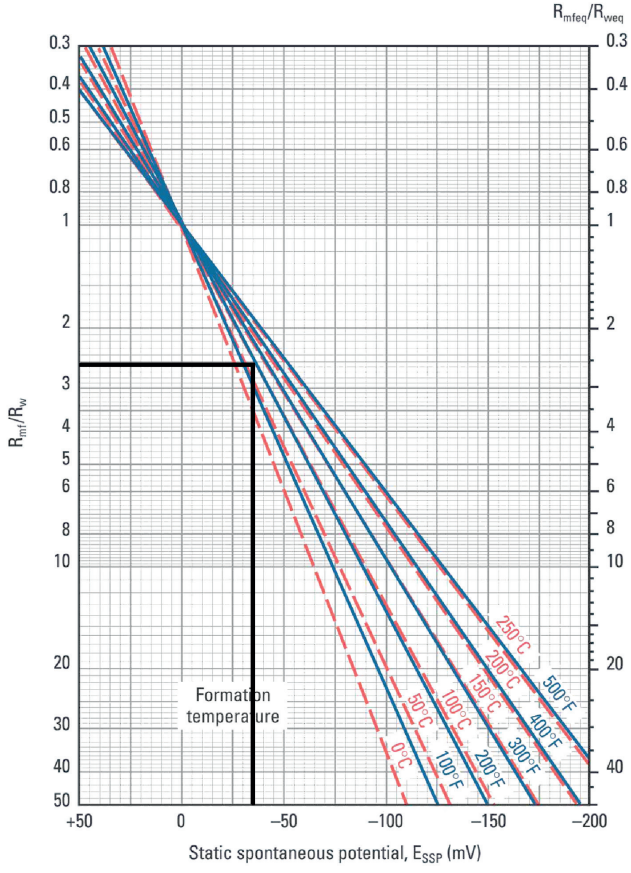

Fig. 5. Determination of R_{mf}/R_{we} based on Self-Potential (Schlumberger, 1977; Zhang et al., 2022c).

consistently pointed to predominantly mixed Type III and mixed Type II/III kerogens. This conclusion was corroborated by S2 versus TOC analysis, which aligned with the interpretation derived from the Van Krevelen diagrams (Figs. 6 and 7).

As organic matter undergoes thermal maturation, characterized by escalating temperature and pressure with depth, the hydrogen-to-carbon ratio experiences a decline. This decline arises from the preferential release of hydrogen-rich volatile compounds, such as methane, in comparison to less hydrogen-rich compounds like

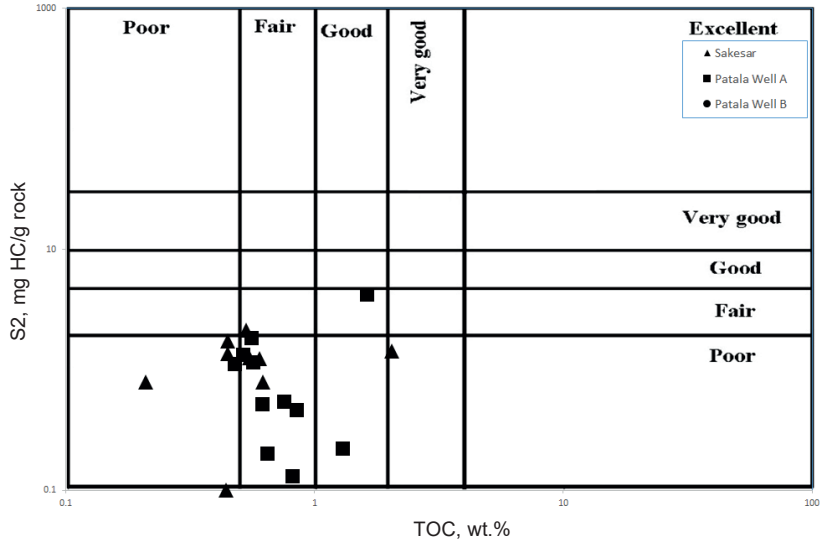

Fig. 6. S2 vs TOC plot.

Table 4. **Various well logs calculated parameters**

Depth, ft.	ΦD	R_t (LLD)	Φ (N.D)	R_w	SP	Temp	R_{we}	RHOB	SH	Sw	Lithology
4058	0.15	320	0.11	0.69	–27	151.8	0.41	2.63	66%	34%	
4075	0.11	300	0.13	0.82	–11	152.1	0.49	2.66	63%	37%	
4093	0.09	160	0.1	0.63	–29	152.9	0.61	2.61	64%	36%	
4110	0.12	900	0.08	0.42	–30	153.3	0.58	2.67	68%	32%	Limestone
4128	0.14	1430	0.14	0.34	–27	153.7	0.27	2.62	61%	39%	
4145	0.07	1680	0.11	0.47	–31	154.1	0.66	2.68	77%	23%	
4163	0.1	450	0.12	0.37	–35	154.4	0.35	2.69	73%	27%	

Table 5. **Measured TOC and Rock-Eval pyrolysis data of all three formations**

No	Depth	Formation	Lithology	TOC, %	S1, mg/g	S2, mg/g	T_{max}, °C	GP, kg/t	PI	HI
1	1270	Nammal	Limestone and shale	0.44	0.32	0.1	407	0.42	0.76	23
2	1290	Nammal	Limestone and shale	0.68	0.21	0.09	409	0.3	0.7	13
3	1300	Nammal	Limestone and shale	2.04	0.85	1.43	411	2.28	0.37	70
4	1320	Nammal	Limestone and shale	0.45	0.35	1.73	424	2.08	0.17	384
5	1340	Nammal	Limestone and shale	0.6	0.25	1.24	427	1.49	0.17	207
6	1350	Nammal	Limestone and shale	0.21	0.14	0.79	420	0.93	0.15	376
7	1360	Nammal	Limestone and shale	0.62	0.17	0.79	422	0.96	0.18	127
8	1390	Nammal	Limestone and shale	0.53	0.39	2.14	422	2.53	0.15	404
9	1430	Dungan	Limestone and shale	0.55	0.1	1.25	426	1.35	0.07	227
10	1445	Dungan	Limestone	0.45	0.19	1.36	427	1.55	0.12	302
11	1450	Dungan	Limestone	0.56	0.27	1.82	426	2.09	0.13	325
12	1455	Ranikot	Shale and limestone	1.63	0.42	4.15	426	4.57	0.09	255
13	1465	Ranikot	Shale and limestone	0.57	0.18	1.15	428	1.33	0.14	202
14	1470	Ranikot	Shale and limestone	0.48	0.34	1.11	419	1.45	0.23	231
15	1475	Ranikot	Shale and limestone	0.52	0.36	1.32	420	1.68	0.21	254
16	1485	Ranikot	Shale and limestone	1.31	0.29	0.22	346	0.51	0.57	17
17	1490	Ranikot	Shale and limestone	0.62	0.29	0.51	404	0.8	0.36	82
18	1495	Ranikot	Shale and limestone	0.85	0.36	0.46	401	0.82	0.44	54
19	1500	Ranikot	Shale and limestone	0.76	0.44	0.54	391	0.98	0.45	71
20	1506	Ranikot	Shale and limestone	0.65	0.19	0.2	385	0.39	0.49	31
21	1510	Ranikot	Shale and limestone	0.82	0.18	0.13	329	0.31	0.58	16

heavy hydrocarbons and carbonaceous residues. In our specific case, these factors have collectively contributed to the observed decrease in HI values. Additionally, when a formation undergoes hydrocarbon expulsion or migration, the extracted hydrocarbons (S1) are reduced, leading to a lower HI value. It is vital to emphasize that HI values, when considered in isolation, provide an incomplete assessment of a sedimentary rock's hydrocarbon potential and maturity. Therefore, they must be interpreted in conjunction with other crucial parameters, including TOC content, Rock-Eval data, and various maturity indicators. This comprehensive approach enables a more thorough understanding of the organic matter and its capacity for hydrocarbon generation.

Furthermore, the determination of thermal maturity is a critical aspect of our analysis. The T_{max} values for the samples ranged from 329 to 428 °C, indicating that these samples have not yet entered the maturity window and are situated within the immature zone. The HI versus T_{max} plot for all three formation samples further confirms their placement within the immature zone (Fig. 7) as part of the thermal maturity analysis.

Hydrocarbon generation potential. The hydrocarbon production potential is profoundly influenced by the organic facies of kerogen distributed within source rocks. This factor significantly determines the types of hydrocarbons generated during thermal maturation and can be assessed through a combination of geochemical and petrological parameters (Liu et al., 2023; Shah et al., 2023a). In this research, we ascertained the organic matter's quality, or kerogen type, within the examined sediments and its consequential impact on hydrocarbon generation primarily through comprehensive geochemical analysis of bulk pyrolysis data.

Our analysis unequivocally reveals that the sediments from all three formations exhibit a notably limited hydrocarbon generation potential. The nature of organic matter and the hydrocarbon-generating capacity of

these sedimentary formations were judiciously assessed using pyrolysis data. According to the criteria established by Hunt (1996) and Shah (2023b), sediments with Hydrogen Index (HI) values below 200 mg HC/g TOC and categorized as kerogen Type III are anticipated to predominantly yield gas. Conversely, samples boasting a TOC exceeding 1 wt.% and HI values surpassing 300 are expected to be conducive to oil generation. In our analyses, the prevailing kerogen type predominantly comprised a blend of Type III and Type II/III kerogens (Figs. 6 and 7). Considering the average TOC content of the analyzed sediments at 0.73%, it is evident that these sediments exhibit limited hydrocarbon-generating potential.

Reservoir potential. In pursuit of a quantitative interpretation of reservoir potential, we employed petrophysical analysis methods to derive critical reservoir parameters. Table 4 presents the computed petrophysical parameters gleaned from the assessment of the Sakesar Formation. The calculated average porosity ranges from 8 to 14%, indicating a reservoir potential spanning from poor to good. As per the criteria outlined by Rider (1986) and Shah et al. (2023a), the computed average water saturation stands at 32.58%, while the hydrocarbon saturation is notably higher at 67.42%. These values collectively suggest an average to good hydrocarbon potential, thus providing a qualitative characterization of the reservoir (Table 1).

CONCLUSIONS

Based on the geochemical and petrophysical evaluation techniques conducted on the source and reservoir rocks (Nammal, Sakesar, Dungan, and Ranikot formations) of the Punjab Platform Basin, the findings can be summarized as follows.

Hydrocarbon Generation Potential:

The investigation of sediments originating from the Nammal, Dungan, and Ranikot formations consistently points to a notable deficiency in generative capacity. This conclusion is substantiated by the observed low values of critical parameters, including S2, HI, and T_{max} (Table 5).

Geochemical Characteristics:

S2 values, ranging from 0.09 to 4.15 mg HC/g rock, alongside HI values spanning from 13 to 404 mg HC/g TOC, collectively signify the presence of a mixed kerogen composition, encompassing Types II/III and Type III.

Thermal Maturity Assessment:

Crucially, the thermal maturity analysis indicates that sediments from the Nammal, Dungan, and Ranikot formations are positioned within the immature window zone. This placement strongly implies a limited potential for these formations to serve as prolific source rocks for hydrocarbon generation.

Reservoir Characteristics:

The outcomes of petrophysical analyses specifically targeting the Sakesar Formation indicate that it possesses an average reservoir quality. Furthermore, the findings suggest an average potential for hydrocarbon production within this formation.

The author is very thankful to University of Malaya, Malaysia for providing lab facilities for this study.

REFERENCES

Abdullah, W.H., Togunwa, O.S., Makeen, Y.M., Hakimi, M.H., Mustapha, K.A., Baharuddin, M.H., Sia, S.-G., Tongkul, F., 2017. Hydrocarbon source potential of Eocene–Miocene sequence of western Sabah, Malaysia. Mar. Pet. Geol. 83, 345–361, doi: 10.1016/j.marpetgeo.2017.02.031.

Asquith, G.B., Krygowski, D., Gibson, C.R., 2004. Basic Well Log Analysis. American Association of Petroleum Geologists, Tulsa, Vol. 16.

Bordenave, M.L., Espitalié, L., Leplat, P., Oudin, J.L., Vandenbroucke, M., 1993. Screening techniques for source rock evaluation, in: Bordenave, M.L. (Ed.), Applied Petroleum Geochemistry. Editions Technip, Paris, pp. 217–278.

Chen, J., Wen, L., Bi, C., Liu, Z., Liu, X., Yin, L., Zheng, W., 2023. Multifractal analysis of temporal and spatial characteristics of earthquakes in Eurasian seismic belt. Open Geosci. 15, doi: 10.1515/geo-2022-0482.

Dang, P., Cui, J., Liu, Q., Li, Y., 2023. Influence of source uncertainty on stochastic ground motion simulation: a case study of the 2022 Mw 6.6 Luding, China, earthquake. Stochastic Environ. Res. Risk Assess. 37, 2943–2960, doi: 10.1007/s00477-023-02427-y.

Hartmann, D.J., Beaumont, E.A., 1999. Predicting reservoir system quality and performance, in: Beaumont, E.A., Foster, N.H. (Eds.), Exploring for Oil and Gas Traps. Treatise of Petroleum Geology. Handbook of Petroleum Geology. AAPG, Tulsa.

He, M., Dong, J., Jin, Z., Liu, C., Xiao, J., Zhang, F., Deng, L., 2021. Pedogenic processes in loess-paleosol sediments: Clues from Li isotopes of leachate in Luochuan loess. Geochim. Cosmochim. Acta 299, 151–162, doi: 10.1016/j.gca.2021.02.021.

Huang, S., Lyu, Y., Sha, H., Xiu, L., 2021. Seismic performance assessment of unsaturated soil slope in different groundwater levels. Landslides 18, 2813–2833, doi: 10.1007/s10346-021-01674-w.

Hunt, J.M., 1996. Petroleum Geochemistry and Geology (2nd ed.). W.H. Freeman and Company, New York.

Kadri, I.B., 1995. Petroleum Geology of Pakistan. Pakistan Petroleum Limited, Karachi, Pakistan.

Li, Q., Song, D., Yuan, C., Nie, W., 2022a. An image recognition method for the deformation area of open-pit rock slopes under variable rainfall. Measurement 188, 110544, doi: 10.1016/j.measurement.2021.110544.

Li, J., Wang, Y., Nguyen, X., Zhuang, X., Li, J., Querol, X., Do, V., 2022b. First insights into mineralogy, geochemistry, and isotopic signatures of the Upper Triassic high-sulfur coals from the Thai Nguyen Coal field, NE Vietnam. Int. J. Coal Geol. 261, 104097, doi: 10.1016/j.coal.2022.104097.

Li, J., Lin, Y., Nguyen, X., Zhuang, X., Li, B., Querol, X., Cordoba, P., 2023a. Enrichment of strategic metals in the Upper Triassic coal from the Nui Hong open-pit mine, Thai Nguyen Coalfield, NE Vietnam. Ore Geol. Rev. 153, 105301, doi: 10.1016/j.oregeorev.2023.105301.

Li, C., Smith, P., Bai, X., Tan, Q., Luo, G., Li, Q., Zhang, S., 2023b. Effects of carbonate minerals and exogenous acids on carbon flux from the chemical weathering of granite and basalt. Global Planet. Change 221, 104053, doi: 10.1016/j.gloplacha.2023.104053.

Liu, Z., Xu, J., Liu, M., Yin, Z., Liu, X., Yin, L., Zheng, W., 2023. Remote sensing and geostatistics in urban water-resource monitoring: a review. Mar. Freshwater Res., 74, 747–765, doi: 10.1071/MF22167.

Ma, S., Qiu, H., Yang, D., Wang, J., Zhu, Y., Tang, B., Cao, M., 2023. Surface multi-hazard effect of underground coal mining. Landslides 20, 39–52, doi: 10.1007/s10346-022-01961-0.

Peng, J., Xu, C., Dai, B., Sun, L., Feng, J., Huang, Q., 2022. Numerical investigation of brittleness effect on strength and microcracking behavior of crystalline rock. Int. J. Geomech. 22, 4022178, doi: 10.1061/(ASCE)GM.1943-5622.0002529.

Peters, K.E., 1986. Guidelines for evaluating petroleum source rock using programmed pyrolysis. AAPG Bull. 70, 318–329, doi: 10.1306/94885688-1704-11D7-8645000102C1865D.

Peters, K.E., Cassa, M.R., 1994. Applied source rock geochemistry, in: Magoon, L.B., Dow, W.G. (Eds.), The Petroleum System – From Source to Trap. AAPG Tulsa, Oklahoma USA, Vol. 60, pp. 93–120.

Quijada, M.F., Steward, R.R., 2007. Petrophysical analysis of well logs from Manitou Lake, Saskatchewan. CREWERS Res. Rep., Vol 19, pp. 1–18.

Ran, C., Bai, X., Tan, Q., Luo, G., Cao, Y., Wu, L., Zhang, S., 2023. Threat of soil formation rate to health of karst ecosystem. Sci. Total Environ. 887, 163911, doi: 10.1016/j.scitotenv.2023.163911.

Raza, H., 1973. Organic Geochemistry and Sedimentology of Petroleum Source Rocks of Indus Basin: Pakistan. Geological Survey Open-File Report.

Raza, H.A., Ahmad, W., Ali, SM., Mujtaba, M., Alam, S., Shafeeq, M., 2008. Hydrocarbon prospects of Punjab platform Pakistan, with special reference to Bikaner-Nagaur Basin of India. Pak. J. Hydrocarb. Res. 18, 1–33.

Ren, C., Yu, J., Liu, S., Yao, W., Zhu, Y., Liu, X., 2022a. A plastic strain-induced damage model of porous rock suitable for different stress paths. Rock Mech. Rock Eng. 55, 1887–1906, doi: 10.1007/s00603-022-02775-1.

Ren, C., Yu, J., Liu, X., Zhang, Z., Cai, Y., 2022b. Cyclic constitutive equations of rock with coupled damage induced by compaction and cracking. Int. J. Min. Sci. Technol. 32, 1153–1165, doi: 10.1016/j.ijmst.2022.06.010.

Ren, C., Yu, J., Zhang, C., Liu, X., Zhu, Y., Yao, W., 2023. Micro–macro approach of anisotropic damage: A semi-analytical constitutive model of porous cracked rock. Eng. Frac. Mech. 290, 109483, doi: 10.1016/j.engfracmech.2023.109483.

Rider, M.H., 1986. The Geological Interpretation of Well Logs. John Wiley and Sons, New York, NY.

Schlumberger Log Interpretation Charts, 1977. Schlumberger Limited. New York.

Shah, S.M.I., 2009. Stratigraphy of Pakistan. Government of Pakistan. Ministry of Petroleum and Natural Resources, Geological Survey of Pakistan. Memoirs of the Geological Survey of Pakistan, Vol. 22.

Shah, S.B.A., 2023a. Evaluation of organic matter in Sakesar and Patala formations in southern and northern Potwar Basin, Pakistan. Pet. Sci. Technol. 41, 2071–2087, doi: 10.1080/10916466.2022.2105360.

Shah, S.B.A., 2023b. Investigation of the hydrocarbon generative potential of Eocene, Cretaceous, and Late Triassic age sequences in the Punjab Platform Basin, Pakistan, using geochemical and petrophysical techniques. Carbonates Evaporites 38, 1–12, doi: 10.1007/s13146-022-00842-w.

Shah, S.B.A., Abdullah, W.H., 2016. Petrophysical properties and hydrocarbon potentiality of Balkassar well 7 in Balkassar oilfield, Potwar Plateau, Pakistan. Bull. Geol. Soc. Malaysia 62 (1), 73–77.

Shah, S.B.A., Abdullah, W.H., 2017. Structural interpretation and hydrocarbon potential of Balkassar oil field, eastern Potwar, Pakistan, using seismic 2D data and petrophysical analysis. J. Geol. Soc. India 90, 323–328, doi: 10.1007/s12594-017-0720-x.

Shah, S.B.A., Shah, S.H.A., 2021. Hydrocarbon generative potential of Cretaceous and Jurassic deposits in the Ahmedpur East Oilfield Subsurface, Punjab Platform, Pakistan. J. Geol. Soc. India 97, 923–926, doi: 10.1007/s12594-021-1792-1.

Shah, S.B.A., Abdullah, W.H., Shuib, M.K., 2019. Petrophysical properties evaluation of Balkassar oilfield, Potwar Plateau, Pakistan: implication for reservoir characterization. Himalayan Geol. 40 (1), 50–57.

Shah, S.B.A., Shah, S.H.A., Jamshed, K., 2023a. An integrated palynofacies, geochemical and petrophysical analysis for characterizing mixed organic-rich carbonate and shale rocks in Potwar Basin, Pakistan: Insights for multisource and reservoir rocks evaluation. J. Pet. Sci. Eng., doi: 10.1016/j.petrol.2022.111236.

Shah, S.B.A., Shah, S.H.A., Nath, Manabendra, 2023b. 1-D Basin modelling, 3-D reservoir mapping and source rock generative potential of Balkassar oilfield, Potwar Basin, Pakistan. Pet. Sci. Technol., doi: 10.1080/10916466.2023.2175866.

Sun, X., Chen, Z., Sun, Z., Wu, S., Guo, K., Dong, Z., Peng, Y., 2023a. High-efficiency utilization of waste shield slurry: A geopolymeric flocculation–filtration–solidification method. Constr. Build. Mater. 387, 131569, doi: 10.1016/j.conbuildmat.2023.131569.

Sun, X., Chen, Z., Guo, K., Fei, J., Dong, Z., Xiong, H., 2023b. Geopolymeric flocculation-solidification of tail slurry of shield tunnelling spoil after sand separation. Constr. Build. Mater. 374, 130954. doi: 10.1016/j.conbuildmat.2023.130954.

Wang, W., Li, D., Tang, X., Du, W., 2023. Seismic fragility and demand hazard analyses for earth slopes incorporating soil property variability. Soil Dyn. Earthquake Eng. 173, 108088, doi: 10.1016/j.soildyn.2023.108088.

Wu, Z., Xu, J., Li, Y., Wang, S., 2022b. Disturbed state concept–based model for the uniaxial strain-softening behavior of fiber-reinforced soil. Int. J. Geomech. 22, 4022092, doi: 10.1061/(ASCE)GM.1943-5622.0002415.

Xiao, D., Liu, M., Li, L., Cai, X., Qin, S., Gao, R., Li, G., 2023. Model for economic evaluation of closed-loop geothermal systems based on net present value. Appl. Therm. Eng. 231, 121008, doi: 10.1016/j.applthermaleng.2023.121008.

Xu, J., Lan, W., Ren, C., Zhou, X., Wang, S., Yuan, J., 2021. Modeling of coupled transfer of water, heat and solute in saline loess considering sodium sulfate crystallization. Cold Reg. Sci. Technol. 189, 103335, doi: 10.1016/j.coldregions.2021.103335.

Xu, Z., Wang, Y., Jiang, S., Fang, C., Liu, L., Wu, K., Chen, Y., 2022a. Impact of input, preservation and dilution on organic matter enrichment in lacustrine rift basin: A case study of lacustrine shale in Dehui Depression of Songliao Basin, NE China. Mar. Petrol. Geol. 135, 105386, doi: 10.1016/j.marpetgeo.2021.105386.

Xu, Z., Li, X., Li, J., Xue, Y., Jiang, S., Liu, L., Sun, Q., 2022b. Characteristics of source rocks and genetic origins of natural gas in deep formations, Gudian depression, Songliao Basin, NE China. ACS Earth Space Chem. 6, 1750–1771, doi: 10.1021/acsearthspacechem.2c00065.

Yang, J., Fu, L., Fu, B., Deng, W., Han, T., 2022. Third-order Padé thermoelastic constants of solid rocks. J. Geophys. Res.: Solid Earth 127, e2022JB024517, doi: 10.1029/2022JB024517.

Yang, D., Qiu, H., Ye, B., Liu, Y., Zhang, J., Zhu, Y., 2023a. Distribution and recurrence of warming-induced retrogressive thaw slumps on the Central Qinghai-Tibet Plateau. J. Geophys. Res.: Earth Surf. 128, e2022JF007047, doi: 10.1029/2022JF007047.

Yang, L., Wang, H., Xu, H., Guo, D., Li, M., 2023b. Experimental study on characteristics of water imbibition and ion diffusion in shale reservoirs. Geoenergy Sci. Eng. 229, 212167, doi: 10.1016/j.geoen.2023.212167.

Yin, L., Wang, L., Ge, L., Tian, J., Yin, Z., Liu, M., Zheng, W., 2023a. Study on the thermospheric density distribution pattern during geomagnetic activity. Appl. Sci. 13, 5564, doi: 10.3390/app13095564.

Yu, J., Zhu, Y., Yao, W., Liu, X., Ren, C., Cai, Y., Tang, X., 2021. Stress relaxation behaviour of marble under cyclic weak disturbance and confining pressures. Measurement 182, 109777, doi: 10.1016/j.measurement.2021.109777.

Yuan, C., Li, Q., Nie, W., Ye, C., 2023. A depth information-based method to enhance rainfall-induced landslide deformation area identification. Measurement 219, 113288, doi: 10.1016/j.measurement.2023.113288.

Zahid, M., Khan, A., ur Rashid, M., Saboor, A., Ahmad, S., 2014. Structural interpretation of Joya Mair oil field, south Potwar, Upper Indus Basin, Pakistan, using 2D seismic data and petrophysical analysis. J. Himalayan Earth Sci. 47 (1), 73–86.

Zhan, C., Dai, Z., Soltanian, M.R., de Barros, F.P.J., 2022. Data-worth analysis for heterogeneous subsurface structure identification with a stochastic deep learning framework. Water Resour. Res. 58, e2022WR033241, doi: 10.1029/2022WR033241.

Zhang, X., Wang, Z., Reimus, P., Ma, F., Soltanian, M.R., Xing, B., Dai, Z., 2022a. Plutonium reactive transport in fractured granite: Multi-species experiments and simulations. Water Res. 224, 119068, doi: 10.1016/j.watres.2022.119068.

Zhang, Y., Luo, J., Zhang, Y., Huang, Y., Cai, X., Yang, J., Zhang, Y., 2022b. Resolution enhancement for large-scale real beam mapping based on adaptive low-rank approximation. IEEE Trans. Geosci. Remote Sens. 60, 1– 21, doi: 10.1109/TGRS.2022.3202073.

Zhang, K., Wang, Z., Chen, G., Zhang, L., Yang, Y., Yao, C., Yao, J., 2022c. Training effective deep reinforcement learning agents for real-time life-cycle production optimization. J. Pet. Sci. Eng. 208, 109766, doi: 10.1016/j.petrol.2021.109766.

Zheng, Z., Zuo, Y., Wen, H., Li, D., Luo, Y., Zhang, J., Zeng, J., 2023. Natural gas characteristics and gas-source comparisons of the lower Triassic Feixianguan formation, Eastern Sichuan basin. Pet. Sci. 20, 1458–1470, doi: 10.1016/j.petsci.2023.02.005.

Zhou, S., Lu, C., Zhu, X., Li, F., 2021a. Preparation and characterization of high-strength geopolymer based on BH-1 lunar soil simulant with low alkali content. Engineering 7, 1631–1645, doi: 10.1016/j.eng.2020.10.016.

Zhou, G., Zhou, X., Song, Y., Xie, D., Wang, L., Yan, G., Wang, H., 2021b. Design of supercontinuum laser hyperspectral light detection and ranging (LiDAR) (SCLaHS LiDAR). Int. J. Remote Sens. 42, 3731–3755, doi: 10.1080/01431161.2021.1880662.

Zhou, G., Li, W., Zhou, X., Tan, Y., Lin, G., Li, X, Deng, R., 2021c. An innovative echo detection system with STM32 gated and PMT adjustable gain for airborne LiDAR. Int. J. Remote Sens. 42, 9187–9211, doi: 10.1080/01431161.2021.1975844.

Zhou, G., Deng, R., Zhou, X., Long, S., Li, W., Lin, G., Li, X., 2021d. Gaussian inflection point selection for LiDAR hidden echo signal decomposition. IEEE Geosci. Remote Sens. Lett. 19, doi: 10.1109/LGRS.2021.3107438.